RSC Advances

PAPER

View Article Online
View Journal | View Issue

Cite this: *RSC Adv.*, 2024, **14**, 26829

Development of a new experimental NMR strategy for covalent cysteine protease inhibitors screening: toward enhanced drug discovery†

Abdelali Chihab,[a] Nabil El Brahmi,[a] Ghanem Hamdoun,[a] Abdelmoula El Abbouchi,[a] Hamza Ghammaz,[b] Nadia Touil,[c] Mostafa Bousmina,[a] Elmostafa El Fahime[b] and Saïd El Kazzouli *[a]

Received 8th July 2024
Accepted 13th August 2024

DOI: 10.1039/d4ra04938a

rsc.li/rsc-advances

In the development of antiviral drugs, proteases and polymerases are among the most important targets. Cysteine proteases, also known as thiol proteases, catalyze the degradation of proteins by cleaving peptide bonds using the nucleophilic thiol group of cysteine. As part of our research, we are examining how cysteine, an essential amino acid found in the active site of the main protease (M^{pro}) enzyme in SARS-CoV-2, interacts with electrophilic groups present in ethacrynic acid (**EA**) and compounds **4**, **6**, and **8** to form sulfur–carbon bonds. Nuclear magnetic resonance (NMR) spectroscopy was used to monitor the reaction rate between cysteine and Michael acceptors. We found that the inhibitory activity of these compounds towards M^{pro} is correlated to their chemical reactivity toward cysteine. This approach may serve as a valuable tool in drug development for detecting potential covalent inhibitors of M^{pro} and other cysteine proteases.

Introduction

Proteases, also known as peptidases, proteinases, or proteolytic enzymes, play an important role in many biological processes of bacteria, viruses, and mammals.[1] Through catalysing scissile bond hydrolysis, these enzymes cleave proteins into smaller fragments.[2] According to their catalytic site, proteases are classified into four major groups; namely serine proteases, aspartic proteases, metalloproteases and cysteine proteases.[3] Cysteine proteases, or thiol proteases, are characterized by an active site comprising a cysteine residue and another critical amino acid, typically histidine. In this last case, histidine functions as a base, facilitating the deprotonation of cysteine's thiol group. This process enhances the nucleophilicity of cysteine, defining a key aspect of the enzymatic activity of cysteine proteases.[4] Papain, discovered in 1873, stands as the pioneering exemplar of cysteine proteases.[4] Various thiol proteases have been isolated and completely characterized since then, including cathepsins,[5] calpain,[6] and 3C-like proteases, known as main proteases M^{pro}.[7] Due to its vital role in coronavirus replication cycle, the M^{pro} ($3CL^{pro}$) has been the subject of extensive research around the world.[8,9] Its conservation among several coronaviruses including SARS-CoV and SARS-CoV-2, along with its distinct and unique cleavage recognition site, make it an attractive target for drug development.[8]

Since the apparition of the COVID-19 pandemic in late 2019, many research teams have focused on developing inhibitors that block the activity of the M^{pro} and thereby, inhibit the SARS-CoV-2 virus, the primary cause of this global health crisis.[10,11] Thus, a multitude of potential inhibitors have been identified, several of which are currently undergoing clinical evaluation.[12] Furthermore, Pfizer had successfully brought Paxlovid, a combination of a M^{pro} inhibitor (nirmatrelvir) and an HIV protease inhibitor (ritonavir), to the market as an approved treatment for COVID-19.[13] Overall, the majority of existing M^{pro} inhibitors are competitive inhibitors that target the active cysteine 145 and form a covalent bond with it.[8,14–17] The strategy of forming a covalent linkage involves the use of electrophilic warheads such as aldehyde,[14] active esters,[18] α-ketoamide[19] and Michael acceptors[20] *etc.*, to form a sulfur–carbon (S–C) covalent bond with the cysteine's thiol as depicted in Fig. 1.

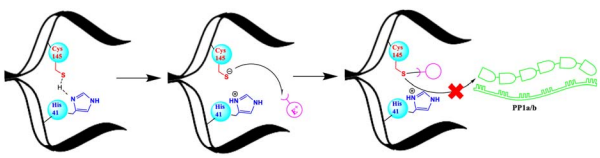

Fig. 1 Schematic representation of the action mode of covalent inhibitors.

[a]*Euromed University of Fes, UEMF, Morocco. E-mail: s.elkazzouli@ueuromed.org*
[b]*Centre National de la Recherche Scientifique et Technique (CNRST), Angle avenues des FAR et Allal El Fassi, Hay Ryad, 10102 Rabat, Morocco*
[c]*Cell Culture Unit, Center of Virology, Infectious, and Tropical Diseases, Mohammed V Military Hospital, Rabat, Morocco*

† Electronic supplementary information (ESI) available. See DOI: https://doi.org/10.1039/d4ra04938a

The formation of the S–C covalent bond with cysteine inhibits its reactivity towards other electrophilic groups, including the scissile bonds within the polyproteins PP1a and PP1b. This inhibition effectively blocks the activity of M^{pro}.[14,16]

Compounds bearing Michael acceptors have been extensively used as potent bioactive molecules in wide range of pharmaceutical applications including anti-inflammatory, antiproliferative and antivirals.[21–23] By strengthening their electrophilicity, their biological and pharmacological properties were improved.[22,24] Moreover, their stability in forming thiol-Michael adducts was found to have a significance impact in their activity of inhibiting kinases.[25]

Presently, bioinformatics plays a crucial role in the advancement of novel drugs, having emerged as an integral element in drug development. Beyond its significance in the examination of various biological components such as genomes, genes, proteins, and enzymes, it serves as a robust screening method facilitating the identification of promising leads exhibiting potent activities.[26,27] There are, however, still some limitations, notably the generation of false positives hits.[28] Therefore, new screening methods are needed to overcome this issue and enhance drug discovery tools.

The present study presents three novel derivatives of **EA**, specifically compounds **4**, **6** and **8**, which exhibit significant inhibitory properties against the SARS-CoV-2 virus. Additionally, the biological evaluation and chemical reactivity analysis of compound **9**, a reduced analogue of compound **8** that lacks the double bond, indicates that the Michael acceptor plays a crucial role in the inhibitory activity within this compound's family. In a subsequent NMR study, we investigate the formation of the S–C covalent bond between the inhibitor and the thiol group of cysteine, a crucial amino acid within the active site of M^{pro} of SARS-CoV and SARS-CoV-2. This study revealed a direct correlation between the inhibitory activity and the chemical reactivity of the corresponding inhibitor towards cysteine. These findings indicate the potential utility of this method in drug development for identifying potent inhibitors of M^{pro} and other cysteine proteases. Beyond its ease of use, this method offers a cost-effective and time-efficient alternative to other screening tools, such as high-throughput screening (HTS), *in vitro* screening, or *in vivo* screening. These conventional methods frequently necessitate expensive equipment, large compound libraries, and extended processing times, as well as complex data interpretation and ethical concerns.[29,30]

Results and discussion

Synthesis

The **EA** derivatives **4**, **6** and **8** were prepared as described in Scheme 1. First, the *N*1-alkylation of 7-nitro-1*H*-idazole **1** was achieved as reported in the literature.[31] Methyl iodide was added to a mixture of **1** with sodium hydride (NaH) in dimethylformamide (DMF) to afford intermediate **2a** in a yield of 86% after stirring at room temperature for 12 h. The analogue **2b** was obtained using the procedure reported by M. Cheung *et al.*[32] **1** reacted with trimethyloxonium tetrafluoroborate ($(CH_3)_3O(BF_4)$) in ethyl acetate (EtOAc) at room temperature to provide **2b** in a yield of 92%. The resulting intermediates **2a** and **2b** were treated with ammonium tetra chloride (NH_4Cl) in a mixture of ethanol/water as solvent to give their corresponding amine intermediates **3** and **5** in quantitative yields (Scheme 1A). This intermediates were reacted in the next step, without any further purification, with **EA** in the presence of *N*-(3-dimethylaminopropyl)-*N*′-ethylcarbodiimide hydrochloride (EDC·HCl) and 1-hydroxybenzotriazole hydrate (HOBt) as activator agents in dichloromethane (DCM) at room temperature overnight to produce the desired products **4** and **6** in 44 and 46% yields, respectively. Reaction of **EA** with the amine **7** under the same conditions afforded compound **8** in a yield of 35% (Scheme 1B).

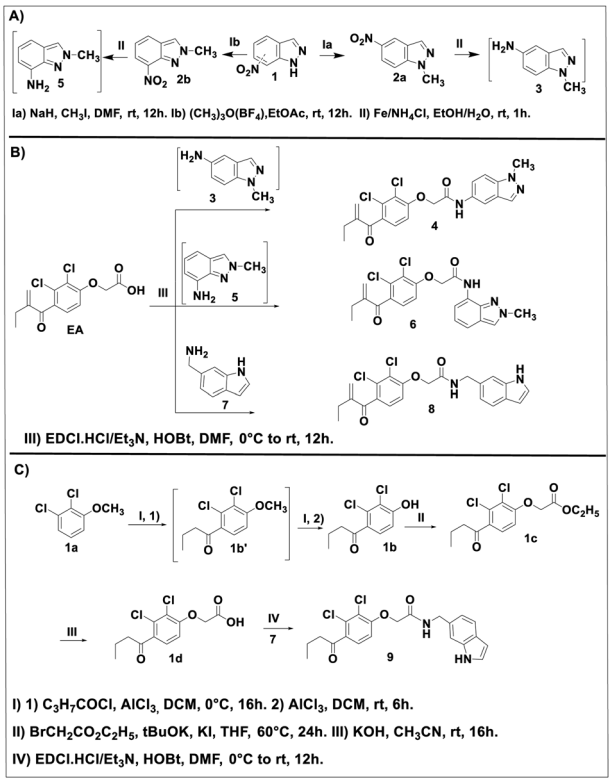

Scheme 1 Synthesis pathway of compounds **4**, **6**, **8** and **9**.

Compound **9**, the reduced analogue of **8** was prepared as described in Scheme 1C, first, a Friedel–Crafts acylation of the anisole **1a** using butyryl chloride was performed to give intermediate **1b**′ which was used in the next step without purification. This step was followed by deprotection of the methoxy group by the action of aluminum chloride ($AlCl_3$) to afford intermediate **1b**. This intermediate underwent a nucleophilic substitution using ethyl-2-bromoacetate in the presence of potassium *tert*-butoxide (*t*BuOK) as base in tetrahydro furane (THF) to afford intermediate **1c** which after basic hydrolysis provided the **EA** reduced analogue **1d**. The same coupling reaction between **1d** and 7 gave compound **9** in a yield of 20%.

Compounds **4**, **6**, **8** and **9** were identified and characterized *via* different characterization techniques, including ^1H and ^{13}C NMR, Fourier-transform infrared spectroscopy (FT-IR), High-resolution mass spectrometry (HRMS), and melting point (MP).

ADMET analysis

The absorption, distribution, metabolism, excretion and toxicity (ADMET) are fundamental parameters that provide valuable information about the drug likeness and the pharmacokinetic properties of a specific lead. They often exhibit as the most challenging part in the drug discovery process. Therefore, we used SwissADME (**http://www.swissadme.ch/**) online tool to predict the ADMET properties of our lead compounds and compare them to **EA** ones which is an already approved drug (Table 1 and Fig. 2).

The investigation of the ADMET properties of our compounds started with an assessment against key drug-likeness criteria derived from Lipinski, Ghose, Veber, and Egan's rules. Notably, all the compounds exhibit clear adherence to all evaluated criteria, suggesting highly favorable pharmacokinetic properties. According to Lipinski's Rule of Five, all the compounds **4**, **6** and **8** demonstrate molecular weight below 500 daltons, a log*P* value under 5, and zero violations for both hydrogen bond donors and acceptors. Ghose's Rule is satisfied, as the compounds falls within the acceptable range for both lipophilicity (log*P*) and molar refractivity. In accordance with Veber's Rule, the compounds display limited number of rotatable bonds and a topological polar surface area (TPSA) of 73.22, 73.22 and 71.19 Å^2 for **4**, **6** and **8**, respectively, which is below the stipulated threshold of TPSA of 140 Å^2. Furthermore, compounds **4**, **6** and **8** fall within the specified range outlined by Egan's Rule, indicating a favorable likelihood of oral bioavailability. Regarding the pharmacokinetic properties, all the studied compounds showed good gastrointestinal (GI) absorption, and no CYP1A2 inhibition except compound **8**. The blood–brain barrier permeability log BB values of −0.704, −0.715, −0.378 for **4**, **6** and **8**, respectively, fall within the range associated with compounds capable of accessing the central nervous system (CNS), in accordance with findings by Santiago Vilar *et al.*[33] In summary the overall ADME profile of the three compounds suggests their potential as viable drug candidates.

Table 1 ADME properties of EA and compounds 4, 6 and 8

Parameters	EA	Comp. 4	Comp. 6	Comp. 8
Molecular weight (g mol^{-1})	303.18	432.30	432.30	431.31
H-bond donors	1	1	1	2
H-bond acceptors	4	4	4	3
Rotatable bonds	6	8	8	9
Molar refractivity	73.67	115.48	115.48	116.05
TPSA (Å^2)	63.60	73.22	73.22	71.19
Bioavailability score	0.85	0.55	0.55	0.55
Lipophilicity (log*P*)	3.61	4.86	4.12	4.49
Solubility (log*S*)	−3.96	−5.39	−5.39	−5.58
GI	High	High	High	High
Log BB	−0.313	−0.704	−0.715	−0.378
P-gp substrate	No	No	No	No
CYP1A2 inhibitor	No	No	No	Yes

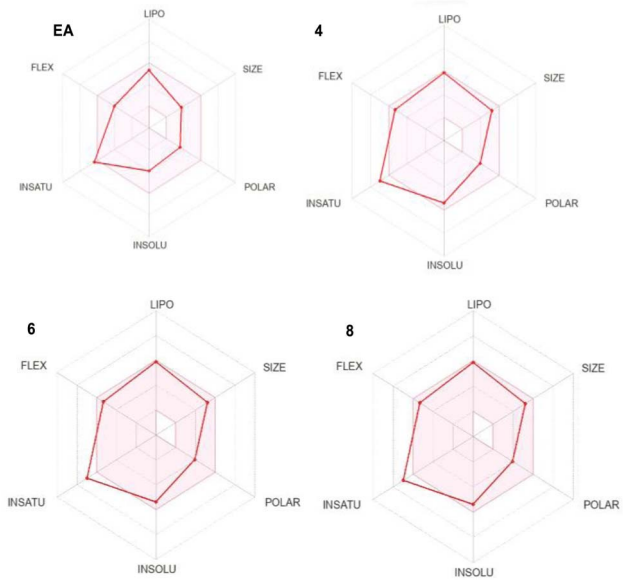

Fig. 2 Bioavailability radar of compound EA, 4, 6 and 8.

Antiviral activity

The SARS-CoV-2 inhibitory activities of compounds **4** and **6** have been evaluated in our previous work.[34] Both compounds exhibited potent activities with EC_{50} value of 3.9 μM for compound **4** and EC_{50} value of 4.8 μM for compound **6**. In our

Table 2 CC_{50} and EC_{50} values of EA, 4, 6, 8 and 9

Comp.	SARS-CoV-2M^{pro} EC_{50} (μM)	CC_{50} (μM)
EA	nd[a]	84 ≥ CC_{50} ≥ 173 lit.[35]
4	3.9	≥50 see ref. 34
6	4.8	≥100 see ref. 34
8	7.8	≥100
9	>100	≥2.5

[a] nd: not determined.

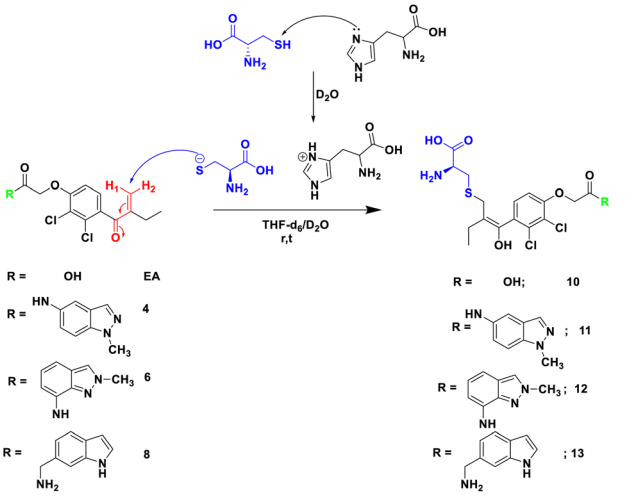

Scheme 2 Reaction of Michael acceptor EA, and its analogues 4, 6 and 8 with cysteine in the presence of histidine as base in THF-d_6/D_2O.

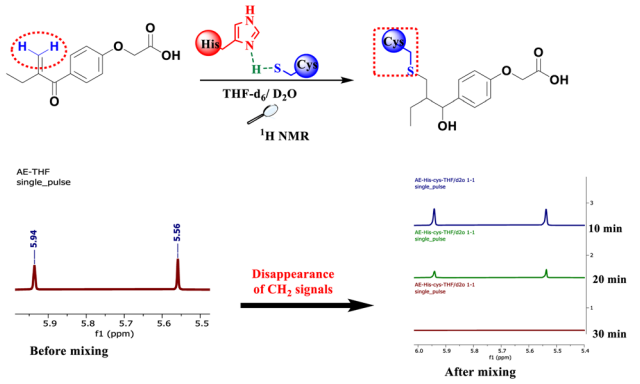

Fig. 3 Evolution of the reaction of **EA** with cysteine in the presence of histidine time.

continuous efforts to discover new SARS-CoV-2 M^{pro} inhibitors, we opted to evaluate the potency of compound **8** and its reduced analogue **9** to inhibit the replication of SARS-CoV-2 *in vitro*. For this purpose, we first conducted cytotoxicity experiments in Vero E6 cells to determine the compound's cytotoxicity. As indicated in Table 2 and Fig. S8,† compound **8** showed no apparent cytotoxicity (CC_{50} > 100 μM). This value is very far from the cytotoxicity concentration as compared to that of the analogue **9** which presented a CC_{50} ≥2 μM. Moreover, As assessed using the quantitative VeroE6 cell-based assay with RNA-qPCR, the medians EC_{50} value of compound **8** is 7.8 μM while that of the analogue **9** exceeds 100 μM (Table 2 and Fig. S8†). This finding highlights the crucial role of the Micheal acceptor moiety in biological activity of this family of compounds.

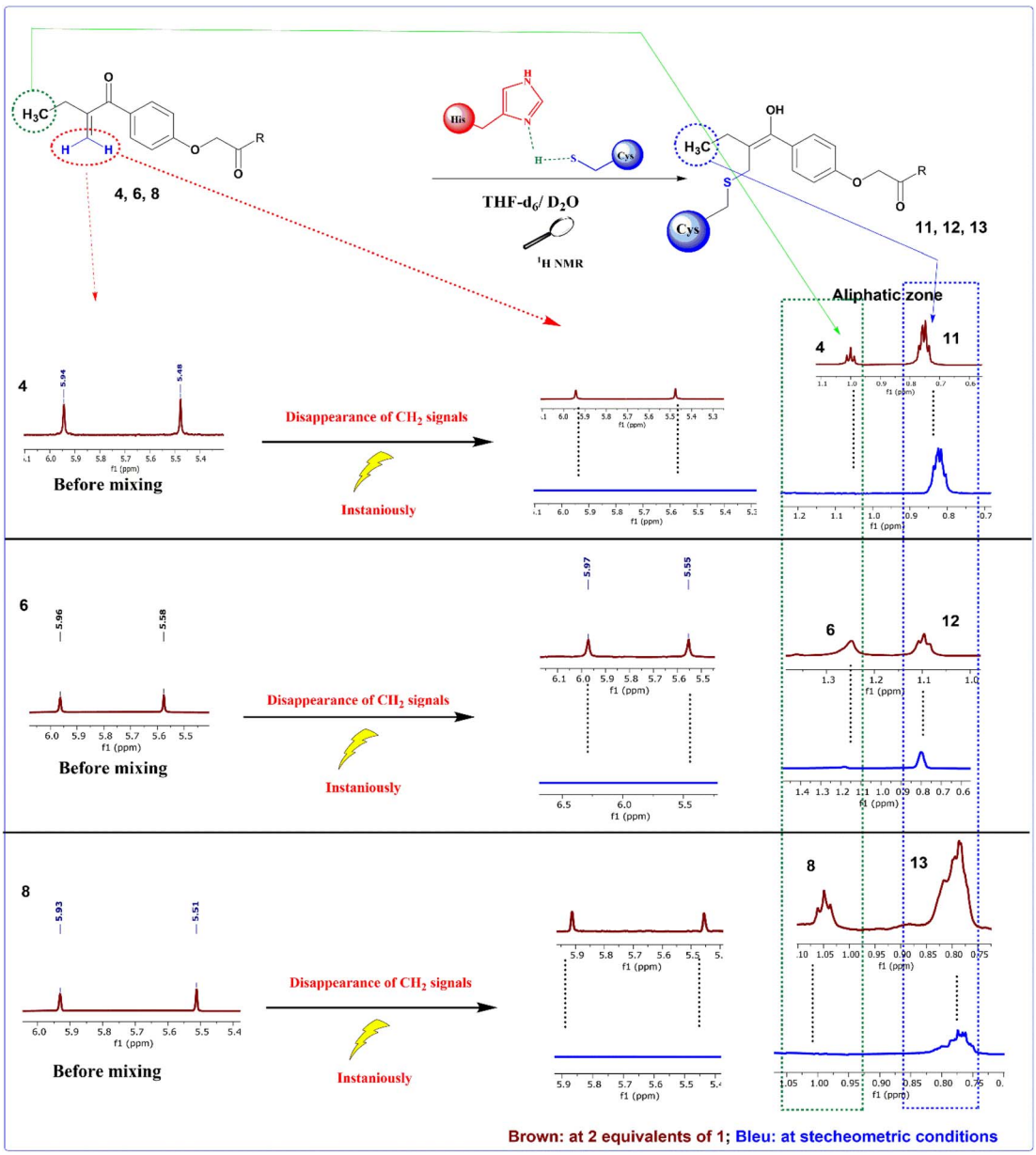

Fig. 4 Instantaneous reactions of **4**, **6** and **8** with cysteine in the presence of histidine.

NMR study

In order to check the ability of **EA**, and its analogues **4**, **6** and **8** to form a S–C covalent bond with cysteine 145 (Cys145), a nucleophilic substitution reaction of these compounds with cysteine in the presence of histidine was carried out, as illustrated in Scheme 2. The formation of the corresponding products **10**, **11**, **12** or **13** in which the sulfur atom of cysteine is covalently linked to the corresponding starting material was monitored and confirmed by NMR spectroscopy.

To mimic the chemical reaction that leads to the covalent bond between Cys145 and the inhibitor, we initially mixed cysteine and histidine, histidine serves as a base to remove the proton from the thiol group, which activated the cysteine, followed by the addition of either **EA**, **4**, **6** or **8**. The reaction was carried out at room temperature in NMR tubes and monitored using a ^{1}H NMR experiment.

As depicted in Fig. 3, before mixing, the β-carbonyl CH_2 of **EA** appears as two separate singlets at 5.56 and 5.94 ppm. These two characteristic singlets of the Michael acceptor were used to follow the evolution of the rection between **EA** and cysteine. After 20 min of reaction, the signals intensity decreases by about 70% due to S–C bond formation and after 30 min all signals of the β-carbonyl CH_2 of **EA** completely disappeared (Fig. 3).

However, when the same process was applied to compounds **4**, **6** and **8**, the reaction with cysteine occurs instantaneously as demonstrated by the immediate disappearance of their characteristic CH_2 signals at 5.48 and 5.94 ppm for compound **4**, 5.58 and 5.96 ppm for compound **6** and 5.51 and 5.93 ppm for compound **8** as depicted in Fig. 4. These reactions were repeated a number of times with varying number of equivalents of the starting materials. The mixtures were analyzed using ^{1}H NMR spectra with 2 equivalents of the related Michael acceptor. The aliphatic zone in Fig. 4 shows both the initial material and its S–C bonded products. Once reaching stoichiometric conditions, the corresponding starting Micheal acceptor disappears immediately.

Compound **9** showed no reaction under the described conditions, confirming that its electrophilic carbonyl center does not react with cysteine to form an S–C covalent bond (Fig. 5).

Carmofur is recognized for its ability to inhibit the SARS-CoV-2 main protease. It covalently alters the Cys145 residue through the formation of a C–S bond.[36] Our investigation, utilizing NMR monitoring, examinates the reactivity of carmofur towards cysteine and its effectiveness in forming a carbon-sulfur covalent bond. As shown by ^{1}H NMR, after 2 h, 75% of the starting carmofur was consumed by cysteine. Carmofur's aromatic doublet at 8.30 ppm totally disappeared after 6 hours, being replaced by the proton signal of the new product **14**, at 7.05 ppm. The reaction rate is, however, slow compared to reactions with **EA** analogues, taking 6 hours to fully consume the starting material, perhaps due to carmofur's reactivity, which could be addressed by further optimization of the reaction parameters (Fig. 6).

Molecular docking

In order to check the ability of the studied compounds to fit into the active site of the M^{pro} and to create favorable interactions

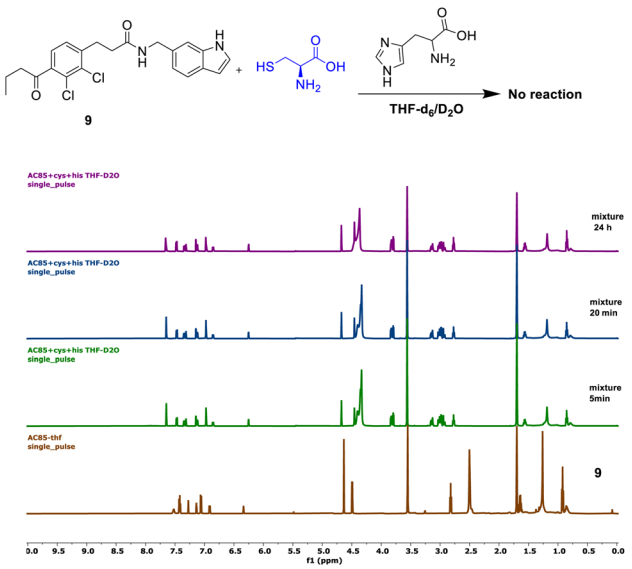

Fig. 5 Investigation of the reactivity of **9** towards cysteine.

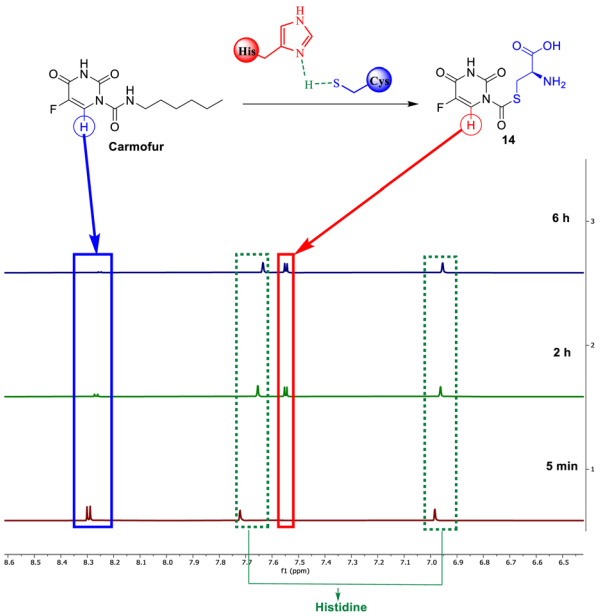

Fig. 6 Reaction of carmofur with cysteine in the presence of histidine.

with the catalytic residues, we performed a molecular docking using the protein M^{pro} (6LU7). Fig. 7 presents the docking score of each compound docked into the enzyme active site as well as, the 3D and 2D visualization of protein-ligand interactions. All the compounds showed good binding energies ranging from −6.5 to −7.3 kcal mol^{-1}. In addition, several interactions have been established with numerous amino acids within the enzyme active site.

Correlation between the chemical reactivity and the biological activity

EA was previously identified as a weak inhibitor of M^{pro}, displaying only approximately 20% inhibition at 100 μM.[37] In

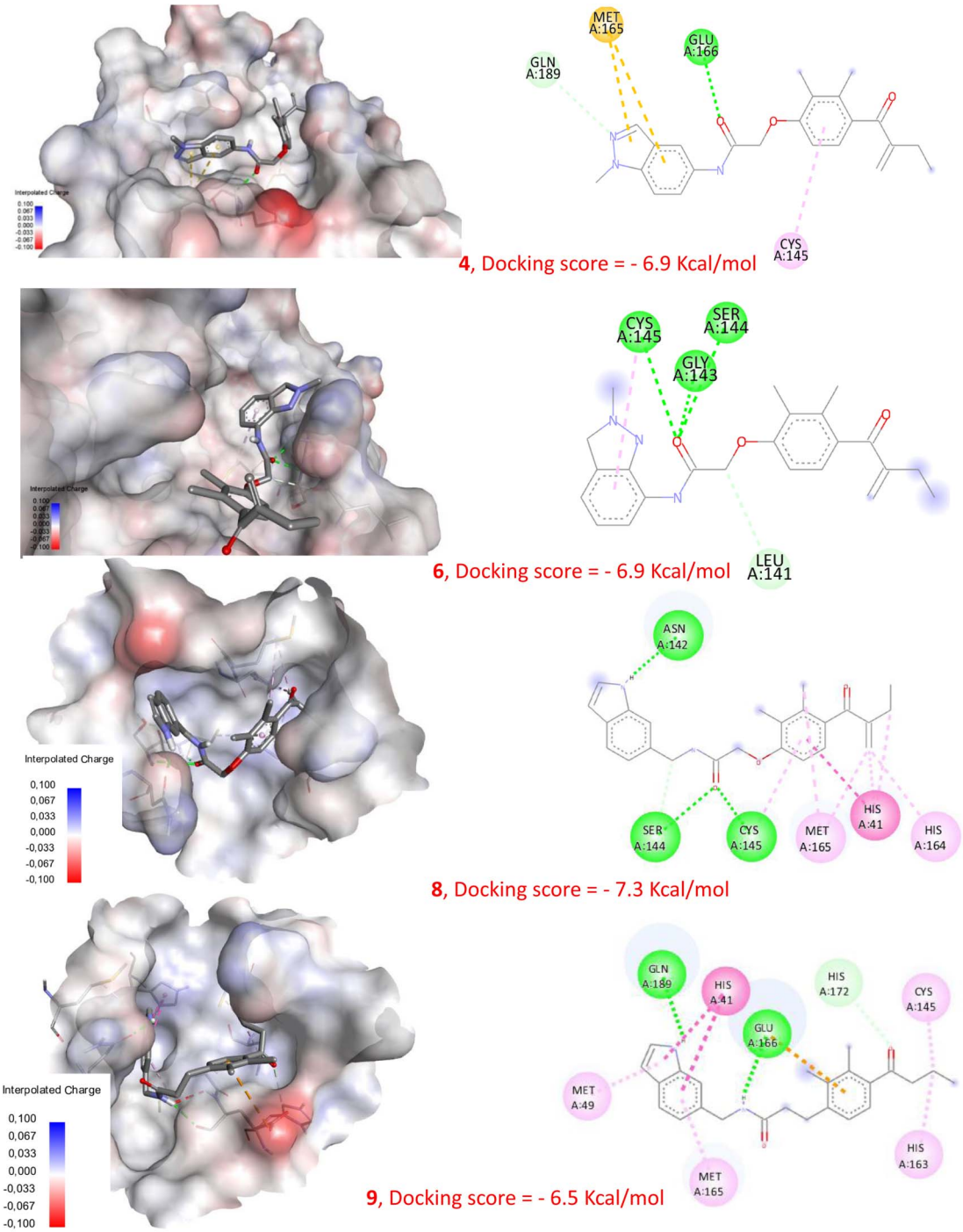

Fig. 7 Molecular docking of compounds **4**, **6**, **8** and **9** with M^{pro} (pdb: 6LU7).

contrast, compounds **4** and **6** exhibited potent inhibitory activity against SARS-CoV-2 M^{pro}.[34] Additionally, compound **8** proved to be an effective SARS-CoV-2 inhibitor, as indicated by its EC_{50} value of 7.8 μM. In addition, compound **9** did not show any inhibitory activity against the virus even at a concentration of 100 μM. Despite these differences in activity, our docking study reveals that all compounds **4**, **6** and **8** displayed the ability to interact with the M^{pro} active site, presenting comparable binding energy values, as illustrated in Fig. 7 and S9.† This highlights that using molecular docking alone can lead to erroneous conclusions by generating false-positive results. However, our new NMR-based approach has demonstrated its ability to rank these compounds according to their reactivity towards cysteine. Indeed, compounds **4**, **6**, and **8** show a remarkably rapid reaction kinetic compared to **EA**, which requires about 30 min for complete conversion of the starting material, and compound **9**, which did not produce any S–C linked derivative. These results indicate that compounds **4**, **6**,

and **8** are highly reactive and capable of forming the expected S–C bond with the catalytic cysteine of M^{pro}, which may explain their significant inhibitory activities. These findings provide further evidence that the biological activity of these compounds is directly related to their chemical reactivity.

Since the majority of M^{pro} inhibitors, as mentioned earlier, are competitive inhibitors that interact with Cys145 through covalent bonding, this new screening method was evaluated using a deferent electrophilic warhead such as the amide group present within the structure of carmofur. As expected, a S–C covalent bond has been formed between carmofur and cysteine which is in accordance with the covalent inhibition mode reported by Z. Jin *et al.*[36]

In light of the findings in this study, an effective screening tool has been formulated. According to this new tool, a good inhibitor candidate should possess at least one of these two properties: (1) forming a sulfur–carbon bond with cysteine or (2) based on the nature of the electrophilic center, the reaction rate can serve as a benchmark for ranking compounds belonging to the same family based on their respective reactivity rates.

Conclusions

This work introduces an innovative screening approach employing NMR spectroscopy to identify a prospective inhibitor for M^{pro} and other cysteine proteases. The method focuses on revealing the formation of S–C bonds between the thiol group of cysteine and the Michael acceptors found in **EA** and its analogues **4**, **6**, and **8**. A reduced analogue of **8**, compound **9**, failed to afford a S–C bond, explaining its poor *in vitro* activity. Accordingly, our new method can be used to identify M^{pro} inhibitors based on their chemical reactivity with cysteine, revealing a direct relationship between inhibitory activity and chemical reactivity. The mechanistic similarity between almost all the cysteine proteases makes our approach applicable to many other protases.

Experimental section

NMR experiments

All ^{1}H NMR measurements were performed using a JEOL 600 MHz spectrometer (with JEOL ROYAL HFX Probe). All spectra were recorded at 29 815 K after 5 min for thermal equilibration.

• Activation of cysteine (mimic of M^{pro}'s active site)

A mixture of histidine (4.5 mg; 0.02 mmol) and cysteine (3.5 mg; 0.02 mmol) was prepared in NMR tube dissolved in 0.7 mL of D_2O to give a neutral solution (pH = 7) (S1).

• Addition of lead inhibitors

✓ Case of **EA**

To the solution S1, a stoichiometric amount of **EA** (8.4 mg; 0.02 mmol), in THF-d_6 was added. The resulting mixture in THF-d6/D_2O (2/1) was then analyzed using ^{1}H NMR experiment at room temperature.

✓ Case of lead compounds **4**, **6** and **8**.

Because of its instantaneous reaction with cysteine (see result and discussion for more Detaille) first 2 equivalents of **4**, **6** or **8** were added to a new S1 solution in NMR tube, a first NMR spectra was obtained. Then, the remaining amount of cysteine and histidine were added to get stoichiometric conditions, this last mixture was analyzed using ^{1}H NMR experiment in the same conditions.

Biological assays

Microneutralization: *in vitro* test for the antiviral activity of molecules. We used a microneutralization assay[38] and which quantitatively assesses whether antibodies or drugs can block SARS-CoV-2 entry and/or replication *in vitro*. For this purpose, microneutralization assays are performed in a 96-well format to ensure medium throughput. Therefore, we have opted for an assay based on RT-PCR by amplification of the genes coding the RNA-dependent polymerase (R) of the virus using the IDV San Sure kit (South Korea). This approach, also used by Gordon *et al.*[39] allows a quantitative assessment of the % inhibition, and therefore, it corroborates the visual observations of the cytopathic effect (CPE).

Screening of the synthesized molecules to evaluate their antiviral effects. The molecules to be tested are solubilized in DMSO according to their molarity. Their cytotoxicity evaluation is mainly based on cell viability determination by means of a fluorescent dye, propidium iodide (logos, Biosystems, USA). It is performed after 24 and 48 hours of incubation with an automatic cell counter integrated with fluorescence optics and image analysis software (Luma, logos, Biosystems, USA).

Determination of the antiviral effect of molecules. The antiviral screening cultures of the molecules are performed in 96-well culture plates. A wider range of concentrations was tested for each of the compounds on VeroE6 cells under the same experimental conditions to determine the effective concentration range, and thus determine an EC_{50} (half maximal Inhibitory Concentration), *i.e.* the dose necessary to obtain 50% inhibition of viral production.

The protocol used follows a prophylactic approach (4 h incubation with 300 $TCID_{50}$ before *in vitro* infection). Indeed, cells are incubated in the presence or absence of the tested compounds for 4 h and then infected at an MOI (Multiplicity of Infection) of 0.01 for duration of 48 h in 37 °C under 5% CO_2.

The effect on viral production (antiviral effect) *in vitro* is measured by RT-qPCR and the determination of infectious titers ($\log TCID_{50}\ mL^{-1}$) is performed on Vero-E6 cells after 48 h of incubation as described by Reed and Muench method (1938). The ratio of the infectious titer in each condition was expressed as a function of the titer measured in the control condition (without treatment).

Docking studies

Protein preparation. The crystal structure of the COVID-19 main protease in complex with the inhibitor N3 (PDB ID: 6LU7) was retrieved from RCSB-PDB database. This protein was prepared by removing water molecules and co-crystallized ligand from the active site of the protein structure. After adding hydrogens and protons the ionizable residues according to the pH of the biological environment, the structure was

corrected for structural errors by addition missing atoms, and then the potential energy was fixed.

Ligands preparation. Each compound was prepared by energy minimization, charge adjustment and followed by a potential energy adaptation using MMFF94 s force field.

Docking. The synthetic molecules were docked at the substrate binding pocket of M^{pro} using AutoDock Vina (version 1.1.2) (active site). The ligand docking simulation was maintained flexible, whereas the protease was made rigid.

Data availability

Source data: crystal structure of SARS-CoV-2 main protease from the protein data bank (**https://www.rcsb.org/**) using the **ID 6LU7** (M^{pro} in complex with inhibitor N3). Software availability: MGLTools: **https://ccsb.scripps.edu/mgltools/downloads/**, AutoDock: **https://autodock.scripps.edu/download-autodock4/**, BIOVIA discovery studio: **https://discover.3ds.com/discovery-studio-visualizer-download**. Underlying data: All the data underlying the results of this study are available as part of this article and ESI.†

Conflicts of interest

There are no conflicts to declare.

Acknowledgements

This research was carried out with the assistance of the Hassan 2 Academy of Sciences and Technologies. The authors are grateful to the Hassan II Academy of Sciences and Techniques and the Euromed University of Fes for funding. The authors are also grateful to the Euromed University of Fes for providing their facilities. AC is grateful for the Euromed University for the scholarship.

References

1 S. Verma, R. Dixit and K. C. Pandey, *Front. Pharmacol*, 2016, **7**, 193290.
2 C. López-Otín and J. S. Bond, *J. Biol. Chem.*, 2008, **283**, 30433.
3 M. B. Rao, A. M. Tanksale, M. S. Ghatge and V. V. Deshpande, *Microbiol. Mol. Biol. Rev.*, 1998, **62**, 597.
4 A. Rawat, M. Roy, A. Jyoti, S. Kaushik, K. Verma and V. K. Srivastava, *Microbiol. Res.*, 2021, **249**, 126784.
5 S. P. M. Lutgens, K. B. J. M. Cleutjens, M. J. A. P. Daemen and S. Heeneman, *FASEB J.*, 2007, **21**, 3029–3041.
6 L. Yu, M. Yin, X. Yang, M. Lu, F. Tang and H. Wang, *Can. J. Physiol. Pharmacol.*, 2018, **96**, 60–67.
7 K. Anand, J. Ziebuhr, P. Wadhwani, J. R. Mesters and R. Hilgenfeld, *Science*, 2003, **300**, 1763–1767.
8 Z. Jin, *et al.*, *Nature*, 2020, **582**, 289–293.
9 L. Zhang, D. Lin, X. Sun, U. Curth, C. Drosten, L. Sauerhering, S. Becker, K. Rox and R. Hilgenfeld, *Science*, 2020, **368**, 409–412.
10 H. Yang and J. Yang, *RSC Med. Chem.*, 2021, **12**, 1026–1036.
11 L. A. Beltrán, S. De La Hoz-Rodríguez, L. B. Iserte, S. Rodríguez, A. Fernández-De-La-pradilla and F. V. González, *Molecules*, 2022, **27**, 2523.
12 B. X. Quan, *et al.*, *Nat. Microbiol.*, 2022, **7**, 716–725.
13 M. Marzi, M. K. Vakil, M. Bahmanyar and E. Zarenezhad, *Biomed Res. Int.*, 2022, **7**, 7341493.
14 W. Dai, *et al.*, *Science*, 2020, **368**, 1331–1335.
15 J. Qiao, *et al.*, *Science*, 2021, **371**, 1374–1378.
16 X. Chen, *et al.*, *Nat. Microbiol.*, 2024, **9**, 1075–1088.
17 G. La Monica, A. Bono, A. Lauria and A. Martorana, *J. Med. Chem.*, 2022, **65**, 12500–12534.
18 S. I. Hattori, *et al.*, *MBio*, 2020, **11**, 1–16.
19 C. Ma, *et al.*, *Cell Res.*, 2020, **30**, 678–692.
20 G. Amendola, *et al.*, *J. Chem. Inf. Model.*, 2021, **61**, 2062–2073.
21 G. Yang, X. Mi, Y. Wang, S. Li, L. Yu, X. huang, S. Tan and H. Yu, *Bioorg. Chem.*, 2023, **134**, 106467.
22 A. El Abbouchi, N. El Brahmi, M. A. Hiebel, H. Ghammaz, E. El Fahime, J. Bignon, G. Guillaumet, F. Suzenet and S. El Kazzouli, *Molecules*, 2023, **28**, 910.
23 M. Liu, B. Xu, Y. Ma, L. Shang, S. Ye and Y. Wang, *Antiviral Res.*, 2021, **192**, 105102.
24 S. T. Liang, C. Chen, R. X. Chen, R. Li, W. L. Chen, G. H. Jiang and L. L. Du, *Front. Pharmacol*, 2022, **13**, 1033003.
25 S. Krishnan, R. M. Miller, B. Tian, R. D. Mullins, M. P. Jacobson and J. Taunton, *J. Am. Chem. Soc.*, 2014, **136**, 12624–12630.
26 O. M. Lage, M. C. Ramos, R. Calisto, E. Almeida, V. Vasconcelos and F. Vicente, *Mar. Drugs*, 2018, **16**, 279.
27 J. P. Hughes, S. S. Rees, S. B. Kalindjian and K. L. Philpott, *Br. J. Pharmacol.*, 2011, **162**, 1239–1249.
28 P. Szymański, M. Markowicz and E. Mikiciuk-Olasik, *Int. J. Mol. Sci.*, 2012, **13**, 427.
29 F. Ver Donck, K. Downes and K. Freson, *J. Thromb. Haemostasis*, 2020, **18**, 1839–1845.
30 X. X. Yang, W. Gu, L. Liang, H. L. Yan, Y. F. Wang, Q. Bi, T. Zhang, J. Yu and G. X. Rao, *RSC Adv.*, 2017, **7**, 3089–3100.
31 M. Naas, S. El Kazzouli, E. M. Essassi, M. Bousmina and G. Guillaumet, *J. Org. Chem.*, 2014, **79**, 7286–7293.
32 M. Cheung, A. Boloor and J. A. Stafford, *J. Org. Chem.*, 2003, **68**, 4093–4095.
33 S. Vilar, M. Chakrabarti and S. Costanzi, *J. Mol. Graphics Modell.*, 2010, **28**, 899–903.
34 S. El Kazzouli, N. Touil, E. El Fahime, A. El Abbouchi, M. Hemlali, N. El Brahmi, A. El Alaoui, S. Bounou and M. Bousmina, *Chinese Pat.*, CN 117730074A, 2024.
35 C. Isgrò, A. M. Sardanelli and L. L. Palese, *Viruses*, 2021, **13**, 106.
36 Z. Jin, *et al.*, *Nat. Struct. Mol. Biol.*, 2020, **27**, 529–532.
37 U. Kaeppler, *et al.*, *J. Med. Chem.*, 2005, **48**, 6832–6842.
38 F. Amanat, *et al.*, *Curr. Protoc. Microbiol.*, 2020, **58**, e108.
39 D. E. Gordon, *et al.*, *Nature*, 2020, **583**, 459–468.